Biomaterials 270 (2021) 120686

Contents lists available at ScienceDirect

Biomaterials

journal homepage: www.elsevier.com/locate/biomaterials

Keto form of curcumin derivatives strongly binds to Aβ oligomers but not fibrils

Daijiro Yanagisawa [a,1], Tomoko Kato [a,1], Hiroyasu Taguchi [a], Nobuaki Shirai [b], Koichi Hirao [c], Takayuki Sogabe [d,2], Takami Tomiyama [e], Keizo Gamo [f], Yukie Hirahara [f], Masaaki Kitada [f], Ikuo Tooyama [a,*]

[a] Molecular Neuroscience Research Center, Shiga University of Medical Science, Seta Tsukinowa-cho, Otsu, 520-2192, Japan
[b] Industrial Research Center of Shiga Prefecture, 232 Kamitoyama, Ritto, 520-3004, Japan
[c] Shiga Prefecture Industrial Support Center, 2-1 Uchidehama, Otsu, 520-0806, Japan
[d] Otsuka Pharmaceutical Co., Ltd, 224-18 Hiraishi Ebisuno, Kawauchi-cho, Tokushima, 771-0182, Japan
[e] Department of Translational Neuroscience, Osaka City University Graduate School of Medicine, 1-4-3 Asahi-machi, Abeno-ku, Osaka, 545-8585, Japan
[f] Department of Anatomy, Kansai Medical University, 2-5-1 Shin-machi, Hirakata, 573-1010, Japan

ARTICLE INFO

Keywords:
Alzheimer's disease
β-amyloid
Oligomer
Curcumin
Keto–enol tautomerism

ABSTRACT

The accumulation of β-amyloid (Aβ) aggregates in the brain occurs early in the progression of Alzheimer's disease (AD), and non-fibrillar soluble Aβ oligomers are particularly neurotoxic. During binding to Aβ fibrils, curcumin, which can exist in an equilibrium state between its keto and enol tautomers, exists predominantly in the enol form, and binding activity of the keto form to Aβ fibrils is much weaker. Here we described the strong binding activity the keto form of curcumin derivative Shiga-Y51 shows for Aβ oligomers and its scant affinity for Aβ fibrils. Furthermore, with imaging mass spectrometry we revealed the blood-brain barrier permeability of Shiga-Y51 and its accumulation in the cerebral cortex and the hippocampus, where Aβ oligomers were mainly localized, in a mouse model of AD. The keto form of curcumin derivatives like Shiga-Y51 could be promising seed compounds to develop imaging probes and therapeutic agents targeting Aβ oligomers in the brain.

1. Introduction

Alzheimer's disease (AD) is characterized by progressive cognitive impairment as a consequence of neuronal and synaptic loss and neurotransmitter deficits. The pathological features of AD are extracellular senile plaques and intracellular neurofibrillary tangles, comprising fibrillar β-amyloid (Aβ) aggregates and hyperphosphorylated tau, respectively [1,2]. The molecular genetics of familial AD supports the amyloid hypothesis; the accumulation of Aβ aggregates in the brain occurs early in the progression of AD [2,3], and Aβ oligomers are particularly neurotoxic [4]. The development of compounds that target Aβ oligomers is thus crucial in the diagnosis and therapeutic treatment of AD.

Curcumin, a low molecular weight yellow-orange pigment in Curcuma longa, reportedly binds to Aβ fibrils and Aβ oligomers in vitro and in vivo [5–8]. Curcumin can exist in an equilibrium state between its keto and enol tautomers. Previously, we found that the curcumin derivatives bound to Aβ fibrils predominantly in the enol form [9], and also demonstrated that the binding activity of the keto form of curcumin derivatives to Aβ fibrils was much weaker [9]. These findings suggested the possibility that the keto form of curcumin derivatives binds to Aβ oligomers.

Here, we synthesized a novel curcumin derivative—Shiga-Y51—with fixed keto forms (Fig. 1), and investigated its binding activity to Aβ oligomers in vitro and in vivo to address this knowledge gap. The results indicated that the keto form of curcumin derivatives holds great potential as an imaging probe and therapeutic agent targeting Aβ oligomers .

* Corresponding author. Molecular Neuroscience Research Center, Shiga University of Medical Science, Seta Tsukinowa-cho, Otsu, 520-2192, Japan.
E-mail address: kinchan@belle.shiga-med.ac.jp (I. Tooyama).
[1] These authors contributed equally to this paper.
[2] Current address: International Office, Tokushima University, 1-1 Minamijosanjima, Tokushima 770–8502, Japan.

https://doi.org/10.1016/j.biomaterials.2021.120686
Received 13 June 2020; Received in revised form 20 December 2020; Accepted 17 January 2021
Available online 23 January 2021

2. Materials and methods

2.1. General methods

We recorded all ^{1}H NMR and ^{19}F NMR spectra on an ECZ-400S 400 MHz NMR spectrometer (JEOL, Tokyo, Japan). We report ^{1}H chemical shifts in ppm (δ) relative to the internal standard, tetramethylsilane (TMS), and chemical shifts in the ^{19}F spectra in ppm (δ) relative to the external standard, C_6F_6, at −163 ppm.

2.2. Preparation of Shiga-Y51

2.2.1. Preparation of 4-methoxymethoxy-3-(trifluoromethoxy)benzaldehyde (II in Fig. 2)

We slowly added chloromethyl methyl ether (1.07 mL, 0.014 mol) to a chilled mixture of 4-hydroxy-3-(trifluoromethoxy)benzaldehyde (2.06 g, 0.01 mol) and potassium carbonate (2.21 g, 0.016 mol) in acetone (18 mL). We stirred the mixture at room temperature for 10 h. We then evaporated the solvent in vacuo, and extracted the residue with ethyl acetate. We washed the extract with water, saturated sodium hydrogen carbonate, and an aqueous sodium chloride solution. After drying the extract over magnesium sulfate, we evaporated the solvent under reduced pressure. We separated the residue chromatographically on silica gel, and collected the fraction eluting in a 1:3 mixture of ethyl acetate and hexane to yield 4-methoxymethoxy-3-(trifluoromethoxy) benzaldehyde (2.48 g, 99%) as a colorless oil.

2.2.2. Preparation of 1,7-bis(4′-methoxymethoxy-3′-trifluoromethoxy) phenyl-4-ethyl-1,6-heptadiene-3,5-dione (III in Fig. 2)

We heated a mixture of 3-ethyl-2,4-pentanedione (256 mg, 2.0 mmol) and boron trioxide (140 mg, 2.0 mmol) in ethyl acetate (4 mL) at 70 °C for 0.5 h. We added tributyl borate (1.08 mL, 4.0 mmol) and a solution of 4-methoxymethoxy-3-trifluoromethoxy)benzaldehyde (1.00 g, 4.0 mmol) to the mixture, and heated it at the same temperature for 0.5 h. We added butylamine (0.20 mL, 2.0 mmol) to the mixture, and then heated it at 70 °C for 5 h. We added hydrochloric acid (2 M, 10 mL) to the mixture after it cooled, and vigorously stirred it for 0.5 h at room temperature. We extracted the mixture with ethyl acetate, and washed the extract with water and aqueous sodium chloride. After drying the extract over magnesium sulfate, we removed the solvent under reduced pressure. We purified the residue via silica gel chromatography, and collected the fraction eluting in a 1:3 mixture of ethyl acetate and hexane. We allowed the fraction to stand at room temperature and solidify. We collected 1,7-Bis(4′-methoxymethoxy-3′-trifluoromethoxy) phenyl-4-ethyl-1,6-heptadiene-3,5-dione (282 mg, 23.9%) following trituration with hexane. Melting point: 124°C-125 °C; ^{19}F NMR ($CDCl_3$): δ-59.50 (s); ^{1}H NMR ($CDCl_3$): δ1.20 (3H, t, $J = 7.2$ Hz), δ2.58 (2H, q, $J = 7.2$ Hz), δ3.50 (6H, s), δ5.26 (4H, s), δ6.96 (2H, d, $J = 15.6$ Hz), δ7.2–7.3 (2H), δ7.4–7.5 (4H), δ7.67 (2H, d, $J = 15.6$ Hz), δ17.38 (1H, s).

2.2.3. Preparation of 1,7-bis(4′-methoxymethoxy-3′-trifluoromethoxy) phenyl-4-ethyl-4-methyl-1,6-heptadiene-3,5-dione (IV in Fig. 2)

We added potassium carbonate (550 mg, 4.0 mmol) to a solution of 1,7-bis(4′-methoxymethoxy-3′-trifluoromethoxy)phenyl-4-ethyl-1,6-heptadiene-3,5-dione (237 mg, 0.40 mmol) and methyl iodide (0.25 mL, 4.0 mmol) in acetone (10 mL), and heated the mixture at 50°C-55 °C for 3 h. We evaporated the solvent in vacuo, and extracted the residue with ethyl acetate. After washing the extract with water and a saturated saline solution, we dried it over magnesium sulfate. We evaporated the solvent under reduced pressure and separated the residue chromatographically on silica gel. From the fraction eluting in a 1:3 mixture of ethyl acetate and hexane we acquired 1,7-bis(4′-methoxymethoxy-3′-trifluoromethoxy)phenyl-4-ethyl-4-methyl-1,6-heptadiene-3,5-dione (230 mg, 95.0%) as a pale yellow oil. ^{19}F NMR ($CDCl_3$): δ-59.59 (s); ^{1}H NMR ($CDCl_3$): δ0.82 (3H, t, $J = 7.2$ Hz), δ1.42 (3H, s), δ2.05 (2H, q, $J = 7.2$ Hz), δ3.46 (6H, s), δ5.23 (4H, s), δ6.65 (2H, d, $J = 15.6$ Hz), δ7.17 (2H, d, $J = 8.4$ Hz), δ7.38 (2H, br, s), δ7.40 (2H, dd, $J = 2$ Hz, 8.4 Hz), δ7.62 (2H, d, $J = 15.6$ Hz).

2.2.4. Preparation of 1,7-bis(4′-hydroxy-3′-trifluoromethoxy)phenyl-4-ethyl-4-methyl-1,6-heptadiene-3,5-dione (Shiga-Y51)

We added 1 M HCl (1.80 mL, 1.80 mmol) to a solution of 1,7-bis(4′-

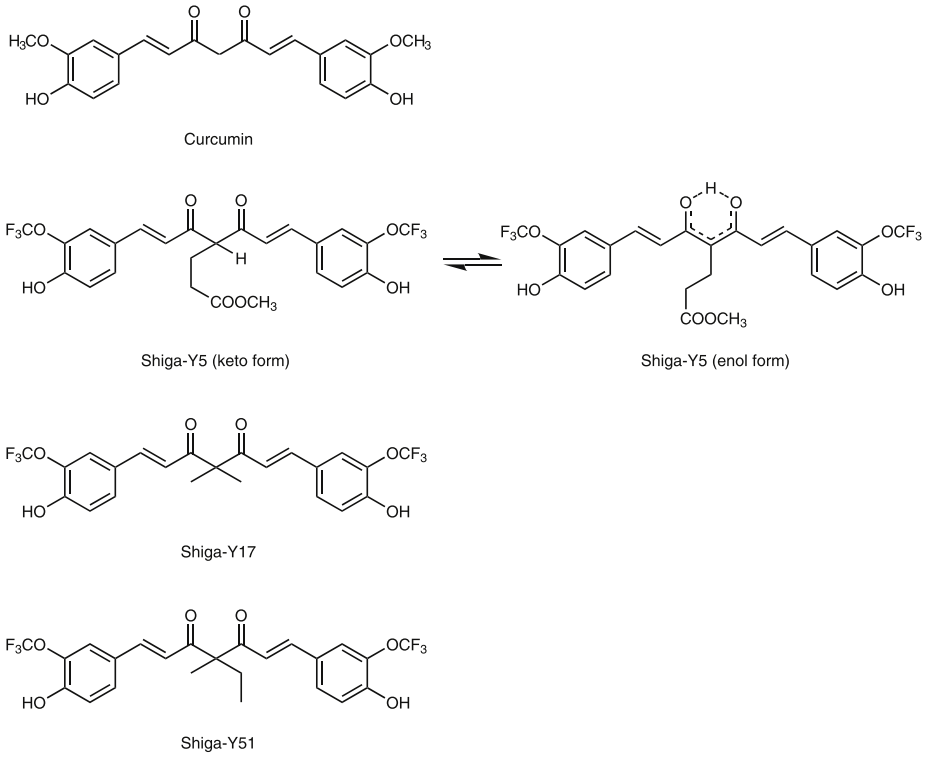

Fig. 1. Chemical structures of Shiga-Y5, Shiga-Y17, and Shiga-Y51.

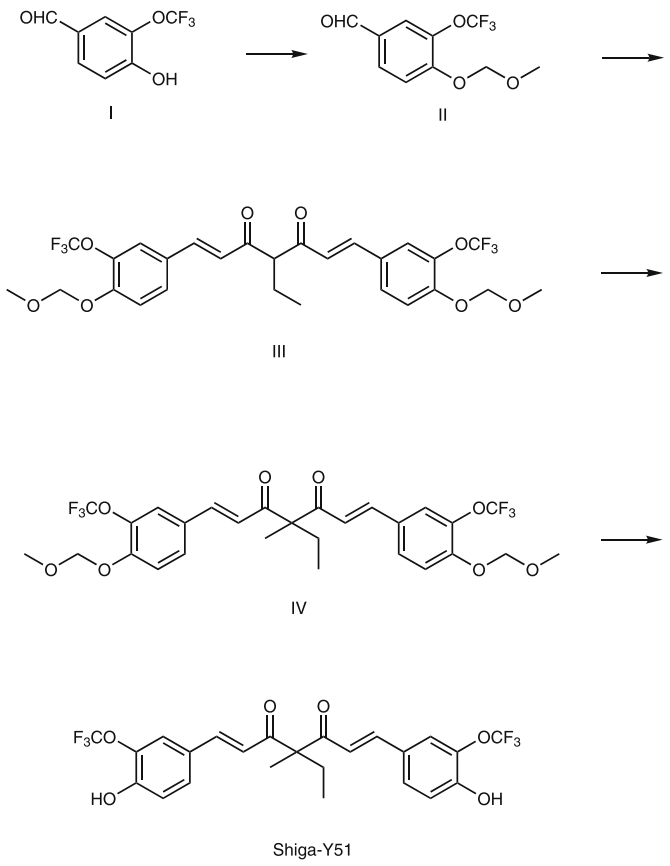

Fig. 2. Preparation of Shiga-Y51. We reacted 4-Hydroxy-3-(trifluoromethoxy) benzaldehyde (I) with chloromethyl methyl ether under basic conditions to protect the phenolic group on the benzaldehyde. We condensed the protected benzaldehyde derivative (II) with 3-ethyl-2,4-pentanedione to obtain the 4-ethyl curcumin derivative (III) using classical methods employed for curcumin synthesis. However, harsher reaction conditions were required to prepare curcumin derivative III than those used for the derivatives without phenolic protecting groups. We introduced the methyl group to compound III by heating it with methyl iodide in acetone under basic conditions. Finally, we removed the methoxymethoxyl group via the acid hydrolysis of derivative IV to obtain 1,7-bis(4′-hydroxy-3′-trifluoromethoxy)phenyl-4-ethyl-4-methyl-1,6-heptadiene-3,5-dione (Shiga-Y51).

methoxymethoxy-3′-trifluoromethoxy)phenyl-4-ethyl-4-methyl-1,6-heptadiene-3,5-dione (182 mg, 0.30 mmol) in ethanol (6.0 mL), and heated the mixture at 60°C-65 °C for 4 h. We evaporated the solvent under reduced pressure, and extracted the residue with ethyl acetate. After washing the extract with water and a saturated saline solution, we dried it over magnesium sulfate. We removed the solvent in vacuo, and separated the residue on a silica gel chromatography column. We collected the fraction eluting in a 1:3 mixture of ethyl acetate and hexane and dissolved it in a small amount of ethyl acetate. We added hexane to the solution to afford 1,7-bis(4′-hydroxy-3′-trifluoromethoxy) phenyl-4-ethyl-4-methyl-1,6-heptadiene-3,5-dione (101 mg, 65%) as colorless crystals. Melting point: 89°C-91 °C; ^{19}F NMR ($CDCl_3$): δ-59.22 (s); ^{1}H NMR ($CDCl_3$): δ0.82 (3H, t, $J = 7.2$ Hz), δ1.42 (3H, s), δ2.05 (2H, q, $J = 7.2$ Hz), δ5.69 (2H, s), δ6.64 (2H, d, $J = 15.6$ Hz), δ7.01 (2H, d, $J = 8.4$ Hz), δ7.35 (2H, br, s), δ7.39 (2H, dd, $J = 2$ Hz, 8.4 Hz), δ7.61 (2H, d, $J = 15.6$ Hz). Because a silica gel thin layer chromatography plate eluted with 1:3 ethyl acetate:hexane showed only one spot, we deemed the material sufficiently pure for use. However, we purified it further by recrystallizing it from a 1:3 mixture of ethyl acetate and *n*-hexane to determine its melting point (90.5°C-91.5 °C).

2.3. Preparation of Aβ aggregates

We prepared Aβ oligomers and fibrils using previously reported protocols [10]. Briefly, we prepared a 1 mM mixture of Aβ1_{-42} peptides (Peptide Institute, Osaka, Japan) in 1,1,1,3,3,3-hexafluoro-2-propanol (HFIP; Wako, Osaka, Japan) and incubated it at 37 °C for 1 h. HFIP broke hydrogen bonds and eliminated pre-existing structural inhomogeneities in the Aβ peptides [11]. We removed the HFIP by evaporation under reduced pressure, and stored the HFIP-treated Aβ peptides at −30 °C. Prior to use, we dissolved the treated Aβ peptides in dimethyl sulfoxide (DMSO) to a concentration of 5 mM. To prepare the Aβ fibrils, we diluted the Aβ solution to 100 μM in 10 mM phosphate-buffered saline (PBS) and incubated it for 48 h at 37 °C. We prepared the Aβ oligomers (globulomers) according to the method reported by Barghorn et al. [12]. We diluted the Aβ peptides dissolved in DMSO at a concentration of 400 μM in PBS with 0.2% sodium dodecyl sulfate (SDS) and incubated them for 6 h at 37 °C. We then diluted the mixture to 100 μM with H_2O and incubated it for 18 h at 37 °C. Following centrifugation at 14,000×*g* for 10 min at 4 °C, we collected the oligomer-enriched supernatant and utilized it for Western blotting and quartz crystal microbalance (QCM) analysis. We confirmed the formation of globulomers by Western blotting, detecting bands in the range from 35 to 50 kDa (Supplementary Fig. 1), and QCM analysis showing significant binding of Shiga-Y5—but no significant binding of ThT—to globulomer-immobilized electrodes.

To prepare intermediate Aβ aggregates with different aggregation periods, we incubated Aβ peptides at 50 μM in PBS at 26 °C with a dry block incubator for 0, 4, 8, and 12 h, and stored at −30 °C before use.

2.4. Western blot analysis

We performed Western blot analysis to confirm aggregation of the Aβ peptides. We then subjected the Aβ aggregates to sodium dodecyl sulfate-polyacrylamide gel electrophoresis (SDS-PAGE) without a reducing agent, and subsequent Western blotting to determine their molecular weight and purity. We diluted the Aβ aggregates to 25 μM and mixed with an equal volume of non-reducing Laemmli buffer (Bio-Rad Laboratories, Hercules, CA, USA) without heating. We separated them via SDS-PAGE in a precast 15% polyacrylamide gel (SuperSep Ace, Wako) at 20 mA for 60 min, thereafter transferring them to Immobilon-P polyvinylidene difluoride (PVDF) membranes (Millipore, Burlington, MA, USA). We blocked the membranes using 5% skim milk in 25 mM Tris-buffered saline (pH 7.4) containing 0.1% Tween-20 (TBS-T) for 60 min. We incubated the blots for 60 min with rabbit polyclonal anti-human Aβ (N-terminal) antibody (1:500; Product code 18584; Immuno-Biological Laboratories, Fujioka, Japan) or mouse monoclonal anti-Aβ E22P antibody [13–15] (clone 11A1; 1:100; Immuno-Biological Laboratories) in TBS-T at room temperature, and then washed them in TBS-T. We incubated the membranes with goat anti-rabbit IgG (H + L) antibody (1:10,000; Thermo Scientific, Rockford, IL, USA) conjugated to horseradish peroxidase, followed by SuperSignal West Pico chemiluminescent substrate (ThermoFisher Scientific, Waltham, MA, USA). We detected the signal using an ImageQuant LAS 4000 system (GE Healthcare, Buckinghamshire, UK).

2.5. Quartz crystal microbalance (QCM) analysis

We determined the binding affinities of Shiga-Y5, Shiga-Y17 and Shiga-Y51 for the Aβ aggregates using an AffinitxQ 27 MHz QCM analyzer (Initium, Tokyo, Japan). The QCM was equipped with a quartz plate 8 mm in diameter and a 4.9 mm^2 Au electrode. We calibrated the quantity of adsorbed compound on the Au electrode surface 20 min after injection to change the frequency by 1 Hz in response to a 0.62 ng increase in mass over a 1 cm^2 area on the electrode. This corresponded to a 1 Hz decrease in frequency for each 30 pg increase in the mass of the 4.9 mm^2 electrode [16]. To immobilize the Aβ fibrils on the electrode, we

placed 2 μL of Aβ fibrils (200 pmol) on the electrode and allowed it to dry for 60 min at RT. To immobilize the Aβ oligomers, we placed 2 μL of the Aβ mixture on the electrode, and stored it overnight at 4 °C in a humid refrigerator, then dried it for 24 h at 4 °C. Prior to QCM analysis, we washed the electrode with water and placed it in the QCM vessel, which contained 8 mL of PBS maintained at 25 °C with stirring at 1000 rpm. After the electrode had stabilized, we added 8 μL of Shiga-Y5, Shiga-17, Shiga-51 and thioflavin T (ThT; Anaspec, Fremont, CA, USA) in DMSO to the reaction vessel. The final concentrations of Shiga-Y5, Shiga-Y17, and Shiga-Y51 were 10 μM each, and the final concentration of ThT was 30 μM. We then recorded the changes in frequency for 20 min.

2.6. Animals

We obtained APPswe/PS1dE9 double transgenic (APP/PS1) mice with a C57BL/6 background from Jackson Laboratory (Bar Harbor, ME, USA). The APP/PS1 mice expressed a chimeric mouse/human amyloid precursor protein (APP) with the K594 N and M595L mutations linked to Swedish familial AD (Mo/HuAPP695swe) and human PS1, carrying the exon 9 deletion associated with familial AD (PS1dE9) [17]. We bred heterozygous males with noncarrier females. We collected ear punches from the offspring, and genotyped the mice using a PCR. We used mice that did not express the transgene as wild-type controls. We housed the mice in standard laboratory cages at 23 °C with free access to water and food, and maintained a 12-h light/dark cycle with the lights on from 8:00 to 20:00. All animal experiments complied with the ARRIVE guidelines, were carried out in accordance with the National Institutes of Health guide for the care and use of Laboratory animals (NIH Publications No. 8023, revised 1978), and were approved by the Animal Care and Use Committee at the Shiga University of Medical Science (Number. 2018-2-12).

2.7. Imaging mass spectrometry

We injected Shiga-Y51 in 10% Cremophor EL (Nacalai Tesque, Kyoto, Japan) into the tail veins of APP/PS1 mice and wild-type mice aged 15–18 months at a dose of 200 mg/kg. We introduced Shiga-Y51 through either bolus injection or continuous injection at a rate of 0.5 mg/kg/mL over 20 min, and deeply anesthetized the mice with sodium pentobarbital at a dose of 50 mg/kg (I.P.). We sacrificed the mice 30 min after the completion of the injection with an overdose of sodium pentobarbital (200 mg/kg), which we injected intraperitoneally. We quickly removed the brains, cut along the sagittal plane, and immersed them in cold 2% carboxymethylcellulose on dry ice. Using a cryostat, we prepared 10 μm brain sections, which we mounted on glass slides coated with indium tin oxide (Matsunami Glass, Kishiwada, Japan).

We vapor-deposited the samples using 9AA as a negative mode matrix under dry vacuum conditions, performing the sublimation of 9AA at 220 °C for 9 min using SVC-700TMSG/7PS80 vacuum vapor deposition equipment (Sanyu Electron, Tokyo, Japan). We performed imaging mass spectrometry using an iMScope matrix-assisted laser desorption/ionization MS (Shimadzu, Kyoto, Japan) in negative reflection mode. To acquire the mass spectra, we scanned the samples using a 1000 Hz Nd:YAG laser with 50 accumulating shots. The detector voltage and sample voltage were 1.66 kV and 3 kV, respectively. We collected spectra over the m/z range from 150 to 600 at a scan pitch of 25 μm, and an intensity of the iMScope laser ranging from 40 to 53. We performed MS/MS analysis to evaluate the target molecules, and verified the spectral data using an iMScope standard sample. We analyzed the data using the Imaging MS Solution™ software package (Shimadzu, Kyoto, Japan).

2.8. Blood-brain barrier permeability of Shiga-Y51

We intravenously injected male wild-type mice at 6.5 months with Shiga-Y51 in 10% Cremophor EL (Nacalai Tesque, Kyoto, Japan) at a dose of 200 mg/kg via bolus injection. We sacrificed the mice 30 min after injection via intraperitoneal injection of an overdose of sodium pentobarbital (200 mg/kg). We quickly removed the brains and stored them at −80 °C until use. We homogenized the brains in methanol, and centrifuged the homogenates at 18,000×g for 10 min at 4 °C. We analyzed the supernatants via LC-MS/MS (QTRAP5500; Sciex, MA, USA) to quantify Shiga-Y51.

2.9. Immunohistochemistry

We fixed the mouse brains of the rest of the IMS study with 4% paraformaldehyde in PB, embedded in paraffin, and sectioned into 5 μm thickness. We deparaffinized the sections and treated them with 0.3% hydrogen peroxide in PBS at RT for 20 min to eliminate endogenous peroxidase activity, thereafter incubating the sections with 70% formic acid solution for 12 min. After several washes with PBS, we heated the sections in 1 mM EDTA (pH8.0) with a microwave oven. After rinsing in PBS, we blocked the sections with 3% BSA in PBS that contained 0.3% Triton X-100 (PBS-T) for 30 min to block non-specific protein binding. We then incubated the sections with rabbit polyclonal anti-human Aβ (N-terminal) antibody (1:200; Product code 18584; Immuno-Biological Laboratories) or mouse monoclonal anti-Aβ E22P antibody (clone 11A1; 1:50; Immuno-Biological Laboratories) in PBS-T containing 0.2% BSA overnight at 4 °C, followed by incubation with biotinylated anti-rabbit IgG (1:1000; Vector Laboratories, Burlingame, CA, USA) or biotinylated anti-mouse IgG (1:2000; Vector Laboratories) for 1 h at room temperature. We then incubated the sections with the avidin-biotin-peroxidase complex (Vectastatin ABC Elite kit, 1:1000; Vector Laboratories) for 1 h. We washed all sections several times with PBS-T between each step, and then revealed labeling by 3,3′-diaminobenzidine (DAB; Dojindo Laboratories, Kumamoto, Japan). We then coverslipped the sections with Entellan (Merck Millipore).

2.10. Fluorescence competition assay

We diluted Aβ fibrils and oligomers prepared as above to 5 μM in PBS, and transferred 100 μL of the Aβ to wells of a black 96-well non-binding plate (Greiner Bio-One, Kremsmünster, Austria). Thereafter, we added test compounds (10 μL of 0.2, 0.6, 2, 6, 20, 60, 200, and 600 μM each in DMSO) to the wells. We diluted curcumin dissolved at 5 mM in DMSO to 5 μM in PBS, and added 90 μL of the solution to each well. After mixing and placing the wells for 30 min at room temperature under dark conditions, we measured the fluorescence with a microplate reader (Infinite M200, Tecan, Zürich, Switzerland) at an excitation wavelength of 430 nm and an emission wavelength of 510 nm for curcumin. We estimated the binding activities to Aβ of the test compounds—expressed as the half-maximal inhibitory concentrations (IC_{50}) with regard to fluorescence—using GraphPad Prism 7 (GraphPad Software, La Jolla, CA, USA).

2.11. Thioflavin T fluorescence assay

We mixed 20 μM Aβ 1–42 peptides in PBS with or without 10 μM Shiga-Y51, and subsequently incubated them in the presence of 5 μM ThT at a total volume of 100 μL in a 96-well black microplate at room temperature. We then measured fluorescence intensity with an excitation of 440 nm and an emission of 485 nm using a microplate reader (Infinite M200; Tecan) with 10 s of agitation every 10 min for 480 min.

2.12. Statistical analysis

We performed statistical analyses using the GraphPad Prism 7 software package (GraphPad Software, La Jolla, CA, USA). We report data as the mean ± the standard error of the mean (SEM). We determined statistical significance with Mann–Whitney tests for single comparisons, and with one-way analysis of variance (ANOVA) followed by Dunnett

tests for multiple comparisons. We considered p-values of <0.05 statistically significant.

3. Results

3.1. Novel curcumin derivatives with fixed keto form

We synthesized the novel curcumin derivative Shiga-Y51, which had methyl and ethyl groups at the C4 position, as a model of a keto form of curcumin derivative (Fig. 1). Here, in addition to Shiga-Y51, we used Shiga-Y5 [9] as a model of a curcumin derivative with keto–enol tautomerism and Shiga-Y17 [9] as another model of a keto form of curcumin derivative.

3.2. Binding activity of curcumin derivatives to Aβ oligomers and fibrils

We prepared the Aβ oligomers and fibrils as reported previously [8] (Supplementary Fig. 1a), and then investigated the interaction of Shiga-Y5, Shiga-Y17 and Shiga-Y51 with Aβ oligomers and fibrils using QCM analysis (Fig. 3; Supplementary Fig. 2). When we added Shiga-Y5 to the QCM vessel at a final concentration of 10 μM, the frequencies of the electrodes on which Aβ fibrils and globulomers were immobilized decreased significantly (Supplementary Fig. 2a and e). In Fig. 3a, e, we compare the quantities of Shiga-Y5 bound to immobilized Aβ fibrils and globulomers on the QCM electrode to those of the control. The addition of Shiga-Y17 (Fig. 3f; Supplementary Fig. 2f) and of Shiga-Y51 (Fig. 3g; Supplementary Fig. 2g) significantly decreased the frequency of the globulomer-immobilized electrode. The addition of Shiga-Y17 significantly reduced the frequency of the fibril-immobilized electrode (Fig. 3b; Supplementary Fig. 2b) and a reduction not induced by Shiga-Y51 (Fig. 3c; Supplementary Fig. 2c). We observed a significant decrease in the frequency of the electrode with immobilized Aβ fibrils after adding thioflavin T (ThT; 30 μM) to the QCM vessel, which is used as an indicator of Aβ fibrils, but in the presence of ThT there was no difference between the control and the electrode with respect to immobilized globulomers (Fig. 3d, h; Supplementary Fig. 2d and h). We calculated quantities of the compounds bound to Aβ oligomers and fibrils over a period of 20 min (Table 1). Shiga-Y51, Shiga-Y17, Shiga-Y5, and ThT were bound to Aβ oligomers and fibrils in molecular ratios of 2.57, 2.52, 1.29, and 0.24, respectively (Table 1). These results indicated that Shiga-Y5 bound to both fibrils and globulomers, whereas ThT bound only to fibrils, as observed previously [8]. In addition, Shiga-Y17 and Shiga-Y51 bound to the globulomers preferentially, showing much lower affinities for the Aβ fibrils.

3.3. QCM analysis of intermediate Aβ aggregates over different aggregation periods

We further investigated whether Shiga-Y51 bound to intermediate Aβ aggregates in the fibrillization process using QCM analysis with electrodes that were mounted with Aβ peptides incubated at 26 °C for 0, 4, 8, and 12 h (Fig. 4; Supplementary Fig. 1B). QCM analysis showed that the most noticeable decrease in frequency was detected in Aβ peptides incubated for 4 h among these samples (Fig. 4a). Furthermore,

Table 1
Quantities of Shiga-Y compounds bound to Aβ oligomers and Aβ fibrils.

Compound	μM	Oligomers (pmol)	Fibrils (pmol)	Oligomer/Fibril
Shiga-Y5	10	71.1	55.1	1.29
Shiga-Y17	10	69.8	27.7	2.52
Shiga-Y51	10	59.5	23.1	2.57
Thioflavin T	30	8.5	35.6	0.24

We calculated the total quantity of Shiga-Y compounds that bound to the control and Aβ-immobilized electrodes after 20 min based on frequency changes. A 1 Hz frequency decrease corresponded to a 30 pg mass increase on the electrode. We quantified the Shiga-Y compounds bound to the oligomers and fibrils by subtracting the total quantity of Shiga-Y compounds bound to the control electrodes from the total quantity bound to oligomers or fibrils that were immobilized on the electrodes.

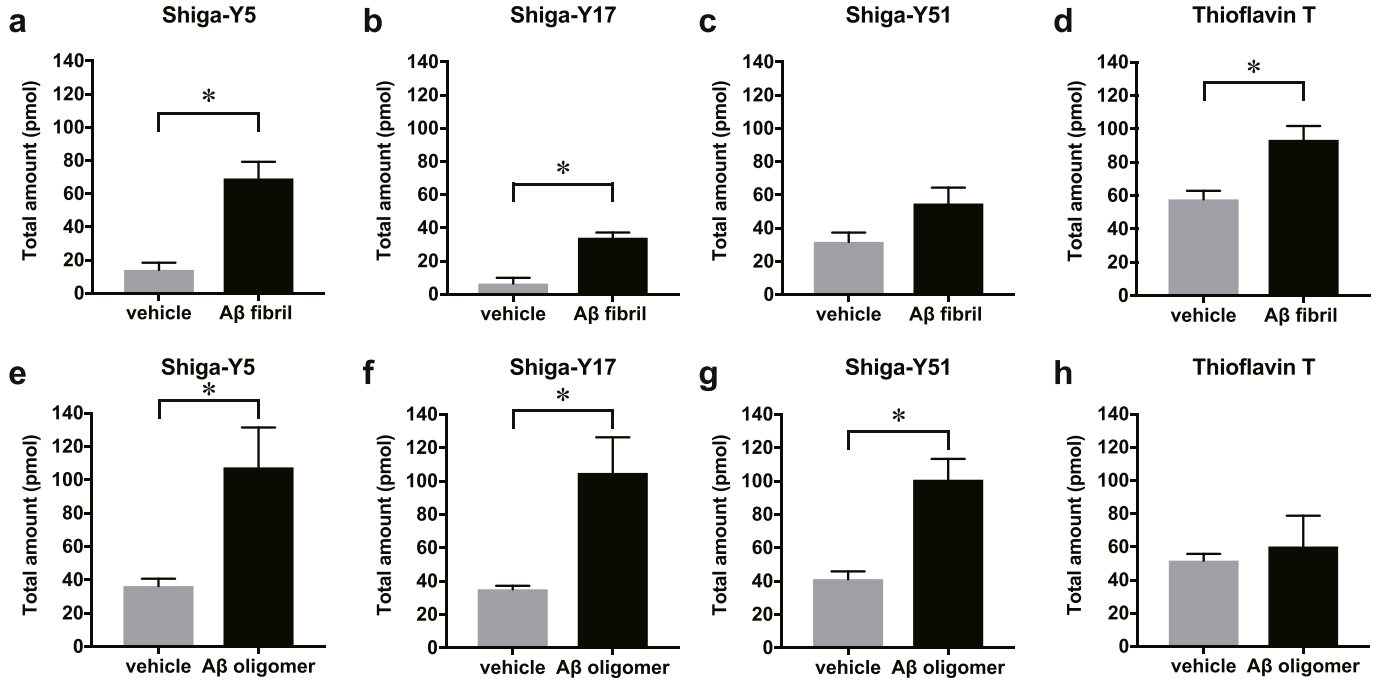

Fig. 3. Total quantity of Shiga-Y compounds bound to Aβ fibrils and Aβ oligomers on the Au-coated QCM sensor. We estimated the quantities of Shiga-Y5 (a,e), Shiga-Y17 (b,f), Shiga-Y51 (c,g), and thioflavin T (d,h) that bound to Aβ fibrils (a–d) and oligomers (e–h) immobilized on the electrodes based on changes in frequency over 20 min. We used solutions without Aβ fibrils and oligomers as controls (gray). The final concentration of each Shiga-Y compound was 10 μM, and the final thioflavin T concentration was 30 μM. We report values from the electrodes with immobilized Aβ fibrils and oligomers as the mean ± SEM of five measurements. We report the control values as the mean of three measurements performed with the electrode alone. Significance (Mann–Whitney test): $^*p < 0.05$.

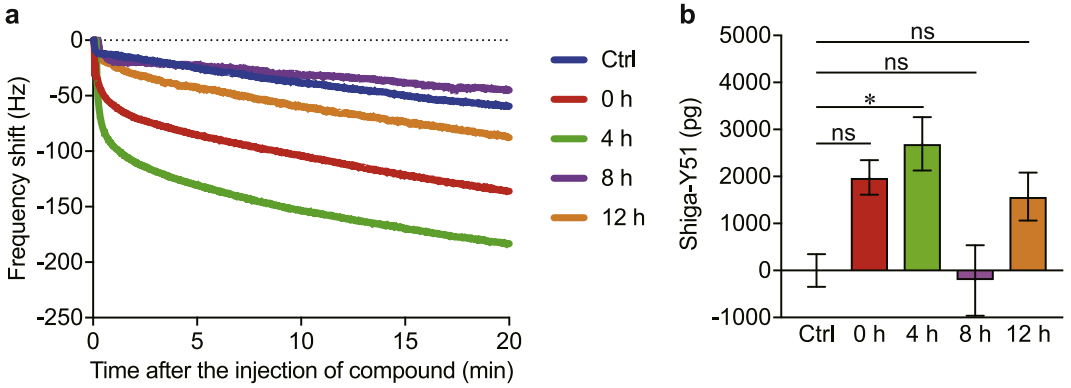

Fig. 4. Shiga-Y51 binds to early-to-intermediate aggregates in the Aβ fibrillization process. (a) Representative frequency changes over 20 min in QCM analysis of Shiga-Y51 with or without (Ctrl) Aβ peptides incubated at 26 °C for 0, 4, 8, and 12 h. (b) The amounts of Shiga-Y51 bound to the electrodes for 20 min in QCM analysis were calculated. Ctrl: control. Data are presented as means ± SEM. Significance was determined by one-way ANOVA followed by a Dunnett test. *$p < 0.05$.

there was a significant increase in the amount of Shiga-Y51 bound to the electrodes with Aβ peptides incubated for 4 h ($p < 0.05$; Fig. 4b), but not with Aβ peptides incubated for 0, 8, and 12 h.

3.4. Shiga-Y51 inhibited the binding of curumin to Aβ globulomers

Next, for further validation of the higher selectivity of Shiga-Y51 for Aβ oligomers over fibrils, we performed fluorescence competition assay. We observed no changes in the fluorescence of curcumin binding to Aβ fibrils in the presence of Shiga-Y51 at concentrations of 0.01–30 μM (Supplementary Fig. 3). In contrast, we observed a dose-dependent decline in the fluorescence of curcumin binding to Aβ oligomers in the presence of Shiga-Y51 (Supplementary Fig. 3). We were unable to obtain the IC_{50} value of Shiga-Y51 with regard to curcumin fluorescence for Aβ fibrils because of the absence of fluorescence inhibition; the IC_{50} value of Shiga-Y51 for Aβ oligomers was 34.61 μM. These results suggest that Shiga-Y51 competes with curcumin binding to Aβ globulomers, but not to Aβ fibrils.

3.5. IMS analysis for the distribution of Shiga-Y51

Our preliminary study detected Shiga-Y51 in the brain extract from the mouse intravenously injected with Shiga-Y51 (Supplementary Table 1), which suggests the brain–blood barrier permeability of Shiga-Y51. To determine in vivo brain distribution of Shiga-Y51, we performed IMS on the mouse brain sections. First, we optimized the method to detect Shiga-Y51 ions using a matrix-assisted laser ionization detection (MALDI) system. We detected standard Shiga-Y51 ions at *m/z* 517.1, and the major fragment of the parent ions (*m/z* 517.1) at *m/z* 229.0 in the tandem mass spectrum (Fig. 5a and b). Next, we performed IMS analysis on brain sections from APP/PS1 mice injected with Shiga-Y51 (200 mg/kg) or vehicle (n = 1 each) via the tail vein. Through IMS analysis, we detected high levels of Shiga-Y51 ions (*m/z* 517.1) and the fragment ions (*m/z* 229.0) in the mouse brain after Shiga-Y51 injection but not after vehicle injection (Fig. 5c–l).

We further investigated the in vivo distribution of Shiga-Y51 in the brains of APP/PS1 mice using IMS. We detected intense signals (*m/z* 517.1) in the cerebral cortex in the brain sections of APP/PS1 mice that were sacrificed 30 min after intravenous injection with Shiga-Y51 (Fig. 5a–c). In contrast, in Shiga-Y51-injected wild-type mice we detected only faint signals in the cerebral cortex (Fig. 5d–f).

3.6. Localization of Aβ oligomers in APP/PS1 mouse brains of APP/PS1 mice

Through immunohistochemical analysis we observed a large number of Aβ deposits mainly in the cerebral cortex, the hippocampus, and the thalamus in the brain of APP/PS1 mice (Fig. 6a). We also detected immunoreactivity for Aβ oligomers using 11A1 antibody in the same regions—namely, the cerebral cortex, hippocampus, and thalamus—in APP/PS1 mice (Fig. 6b).

To investigate the correlation between the distributions of Shiga-Y51 and oligomers, we measured signal intensities of the parent ion at *m/z* 517.1 in IMS analysis and 11A1-immunoreactive areas in the cerebral cortex, hippocampus, hypothalamus, striatum, and corpus callosum. With Pearson's correlation analysis we revealed significant correlation between the signal intensity of Shiga-Y51 in IMS analysis and 11A1-immunoreactivity ($p < 0.05$; Fig. 6e).

3.7. Effects of Shiga-Y51 on the formation of oligomers and fibrils

Finally, we investigated whether Shiga-Y51 affected the formation of Aβ oligomers and fibrils. Western blotting showed no obvious changes in bands of Aβ globulomers that formed in the presence or absence of 50 μM Shiga-Y51 (Supplementary Fig. 4). For Aβ fibril formation, time-course analysis of changes in fluorescence intensity of ThT showed a time-dependent increase in ThT fluorescence when Aβ peptides were incubated in the absence of Shiga-Y51 (Supplementary Fig. 5). In contrast, the increase in ThT fluorescence was inhibited when Aβ peptides were incubated in the presence of 10 μM Shiga-Y51 (Supplementary Fig. 5). These results suggest that Shiga-Y51 may inhibit the formation of Aβ fibrils by interacting with Aβ peptides at the early phase of Aβ aggregation when Aβ fibrils have not yet been formed, but has no effect on the formation of Aβ oligomers.

4. Discussion

In the present study, we showed that a novel curcumin derivative with a fixed keto form—Shiga-Y51—bound to Aβ oligomers in QCM analysis. Comparing the ratios of quantities of compounds binding to Aβ oligomers with those binding to Aβ fibrils, Shiga-Y51 had a relatively high selectivity to Aβ oligomers. Furthermore, IMS analysis demonstrated that Shiga-Y51 passed the BBB, and bound to Aβ aggregates in the brains of APP/PS1 mice after an intravenous injection. These results suggest the potential of Shiga-Y51 as a seed compound targeting Aβ oligomers in the brain.

Our previous study showed that curcumin and the derivatives with keto–enol tautomerism bound to Aβ fibrils in the enol form, and that the binding activity of the keto form to Aβ fibrils was much weaker [9]. In contrast, the present study revealed that Shiga-Y17 and Shiga-Y51—which are curcumin derivatives with fixed keto form—bound strongly to Aβ oligomers, and very weakly to Aβ fibrils in QCM analysis. Furthermore, QCM analysis showed a significant increase in the amount of Shiga-Y51 bound to Aβ peptides that were incubated in PBS for 4 h, but

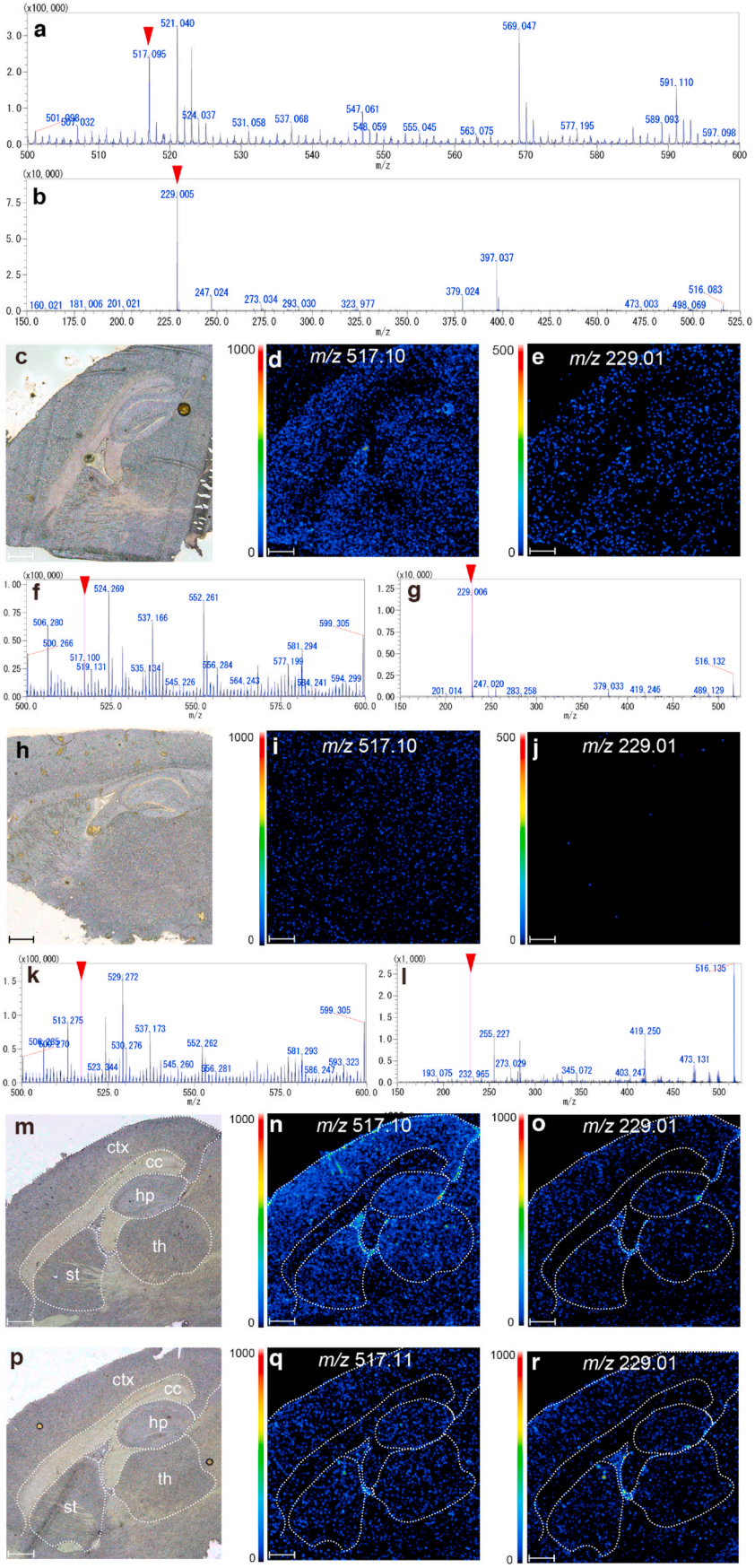

Fig. 5. Imaging mass spectra (IMS) of brain sections from mice injected with Shiga-Y51. (a,b) We detected the Shiga-Y51 ion at *m/z* 517.1 using a matrix-assisted laser ionization detection (MALDI) system. (a) MS spectrum of a Shiga-Y51 standard and (b) the tandem mass spectrum. The major fragment of the parent ion (*m/z* 517.1) detected at *m/z* 229.0 is indicated by the red arrow in (b). IMS imaging analysis and MALDI-MS spectra of brain sections from APP/PS1 mice that received an intravenous bolus injection of (c–g) Shiga-Y51 (200 mg/kg) or (h–l) a vehicle. We show optical images in (c) and (h). IMS images of (d) the Shiga-Y51 parent ion (*m/z* 517.1) and (e) the fragment ion (*m/z* 229.0) show intense signals in the cerebral cortex and hippocampus of an APP/PS1 mouse injected with Shiga-Y51. Only weak signals are visible in the IMS images of a mouse injected with the vehicle (h–l). IMS images of brain sections from (m–o) APP/PS1 and (p–r) wild-type mice after receiving a continuous intravenous injection of Shiga-Y51 (200 mg/kg, 0.5 mL/kg/min). IMS images of (n,q) the parent ion at *m/z* 517.1 and (o,r) the fragment ion at *m/z* 229.0. Signals from the cerebral cortex and hippocampus in the IMS image (*m/z* 517.1) of an APP/PS1 mouse brain section (n) are more intense than those from a wild-type mouse brain (q). Optical images are shown in (m) and (p). ctx, cerebral cortex; hp, hippocampus; th, thalamus; st, striatum; cc, corpus callosum. Scale bar: 600 μm.

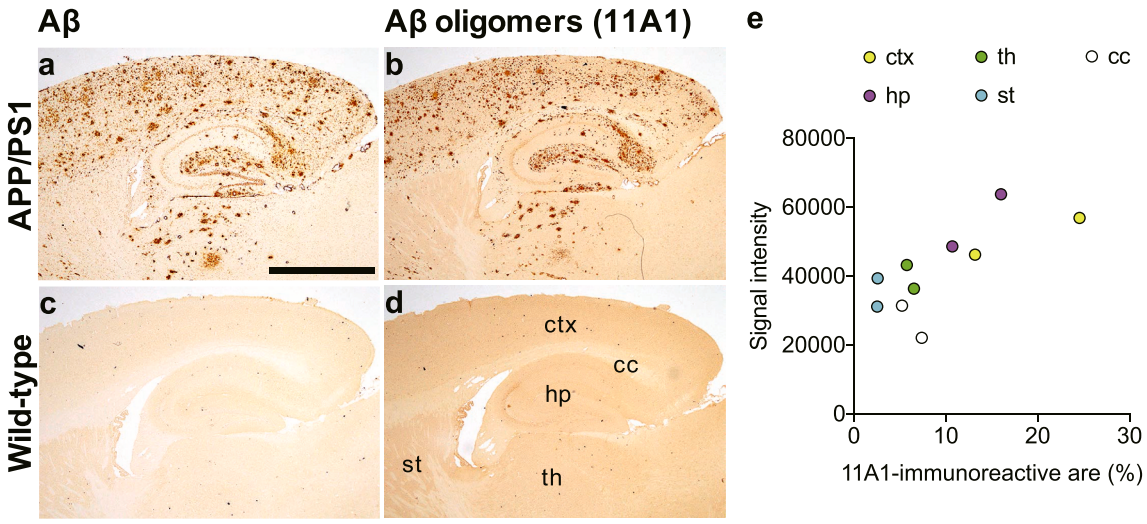

Fig. 6. Immunohistochemical analysis for Aβ oligomers in the brain of APP/PS1 mice. Representative photographs showing immunohistochemistry for Aβ (a,c) and Aβ oligomers that was detected with anti-Aβ E22P antibody (clone 11A1; b,d) in APP/PS1 (a,b) and wild-type mice (c,d). Scale bar: 1 mm. (e) Pearson's correlation analysis revealed significant correlation of 11A1-immunoreactive areas and signal intensities of IMS analysis in the cerebral cortex (ctx), hippocampus (hp), thalamus (th), striatum (st), and corpus callosum (cc) in APP/PS1 mice (n = 2) ($p < 0.05$).

not for 8 and 12 h, suggests that Shiga-Y51 has binding activity against early-intermediate Aβ aggregates in the fibrillization process, and not to later aggregates. These findings suggest that the keto form, rather than the enol form, may be the binding form of curcumin derivatives to Aβ oligomers, which implies the promise of curcumin derivatives with fixed keto form as agents targeting Aβ oligomers.

Entropy-driven processes are well known to play important roles in the formation of the three-dimensional structure of water soluble proteins. That is, in a medium surrounded by water molecules, the hydrophobic amino acid residues tend to move inside of the protein molecule in order to avoid contact with water. This process is possible for proteins because they comprise long chains of amino acids. However, peptides such as Aβ cannot follow this process, because their amino acid chains are not long enough for extensive folding. Aggregation of Aβ seems to be necessary for such peptides containing hydrophobic amino acid residues in avoiding contact of these residues with water. Consequently these peptides form oligomers (such as dimers, trimers, tetramers, and so on). The Aβ oligomer is such a structure, as was recently confirmed by scanning tunneling microscopy [18]. Moreover, Irie proposed the possible structures of small oligomers, and indicated the hydrophobic nature of the cores in these oligomers [19]. The polypeptides in Aβ oligomers appear to bind to each other using their hydrophobic amino acid residues to form hydrophobic cores, and to incorporate hydrophobic molecules into their cores.

Many PET imaging probes—including PiB, flutemetamol, florbetaben, and florbetapir—have been developed for senile plaques which are formed by the aggregation of Aβ fibrils [20]. These probes seem to have a common feature—that is, a ring system which is co-planar and possesses π-electrons which are delocalized in the rings, and move freely within the them. These molecules are therefore flat and rather rigid, and seem to bind to Aβ fibrils easily, but have some difficulty entering the hydrophobic core of Aβ oligomers, because of their rigidity.

However, suitable sized hydrophobic molecules with flexible structures could be incorporated within the hydrophobic core of Aβ oligomers. If this hypothesis is correct, it is reasonable to state that the rather flexible molecules Shiga-Y17 and Shiga-Y51 (see Fig. 1) will bind readily to Aβ oligomers. The binding of Shiga-Y5 to both Aβ fibrils and Aβ oligomers is easily understood, because it is an equilibrium (tautomeric) mixture of keto- and enol-forms (see Fig. 1)—its rather rigid enol form binding to Aβ fibrils and the more flexible keto form binding to Aβ oligomers. Our experimental results are consistent with these statements.

Although in clinical trials many attempts to target Aβ have failed, the human monoclonal antibody Aducanumab recently displayed significant efficacy in Alzheimer phase 3 trials [21,22]. Since Aducanumab targets both Aβ fibrils and soluble Aβ oligomers, it has been suggested that Aβ oligomers play a central role in AD pathogenesis [21,22]. Accordingly, evaluation of Aβ oligomer levels in the in vivo brain would be of great importance in monitoring disease progression in AD. Previous studies, such as BoDipy-Oligomer (BD-Oligo) [23], F-SLOH [24], CRANAD-102 [25], PTO-29 [26], and DCM-AN [27], have reported several near infrared fluorescent imaging probes that selectively labeled Aβ oligomers in the in vivo brain. In the present study, Shiga-Y51 accumulated in APP/PS1 mice after systemic injection, suggesting curcumin derivatives with a fixed keto form as a potential seed structure for imaging probes targeting Aβ oligomers. Further study aimed at the synthesis of derivatives with greater selectivity to Aβ oligomers—and their development as an imaging probe for PET or other modalities—would be of great interest.

In the present study, we found no inhibitory effects on the formations of Aβ oligomers. In contrast, regarding Aβ fibril formation, the increase in ThT fluorescence was inhibited when Aβ peptides were incubated with Shiga-Y51. This result suggests that Shiga-Y51 may inhibit the formation of Aβ fibrils by interacting with Aβ peptides at the early phase of Aβ aggregation when Aβ fibrils have not yet been formed. However, there is also a possibility that, at β-sheeted structures, Shiga-Y51 competes with ThT binding to Aβ fibrils, which may also lead to a decrease in ThT fluorescence. It would therefore be difficult to draw conclusions as to the effects of Shiga-Y51 on the formations of Aβ oligomers and fibrils, based only on limited experiments. Further study aiming to reveal the therapeutic effect of Shiga-Y51 in inhibiting the formation of Aβ oligomers and fibrils remains the aim of future work.

Our study suffered from some limitations. First, we used globulomers [12], which were prepared from synthetic Aβ 1–42 peptides to serve as a model of Aβ oligomers. However, various species of Aβ oligomers differ in size, secondary structure, and cytotoxicity [28,29]. Therefore, it is still unclear whether Shiga-Y51 binds to globulomers specifically or Aβ oligomers in general. Second, we used APP/PS1 mice, in which Aβ oligomers and fibrils accumulate in the same region of the brain. It is therefore quite challenging to demonstrate whether Shiga-Y5 binds specifically to Aβ oligomers in the brains of APP/PS1 mice. We next plan to use APP E693Δ (Osaka mutation) transgenic mice—which show

predominant accumulation of Aβ oligomers in the brain—to demonstrate the in vivo binding of Shiga-Y51 to Aβ oligomers. Lastly, to support the theory that the enol form of curcumin derivatives binds to Aβ fibrils and the keto form binds to Aβ oligomers, it might be interesting to investigate whether the enol form is able to bind to Aβ oligomers. We were unable to investigate this question, because, due to the chemical properties of the curcumin derivative with fixed enol form, it was not easy to perform QCM analysis.

5. Conclusions

Here we demonstrated the binding activity of Shiga-Y51 to Aβ oligomers. In addition, Shiga-Y51 showed BBB permeability and in vivo binding to Aβ aggregates in the brain of an AD mouse model. Detecting Aβ oligomers in the in vivo brain would be critically important in understanding the etiology of AD. Furthermore, considering the recent failures of clinical trials targeting Aβ monomers, targeting Aβ oligomers has become attractive as a therapeutic approach in AD. Therefore, although further efforts are needed, Shiga-Y51 is a first-generation compound targeting Aβ oligomers.

Author contributions

I.T. conceived and designed the project. D.Y. and T.K. performed the experiments related to QCM analysis and administration of Shiga-Y compounds to animals. H.T. synthesized Shiga-Y compounds. T.S. analyzed BBB permeability of the chemicals. N.H. and N.S. examined binding assay of Shiga-Y compounds to amyloid aggregates. T.T. established a transgenic mouse model and offered them to this study. K. G., Y·H., and M.K. performed the experiments related to MS microscopic analysis. D.Y., T.K., H.T., and I.T. wrote and edited the manuscript. All authors contributed to the manuscript revision and read and approved the submitted version of the manuscript.

Declaration of competing interest

The authors declare the following financial interests/personal relationships which may be considered as potential competing interests: T. S. was an employee of Otsuka Pharmaceutical until August 2019. The authors declare no other competing interests.

Acknowledgments

This study was supported by JSPS KAKENHI Grant Numbers JP19K20670 (T.K.), JP19K12780 (H.T.) and JP17H03560 (I.T.).

Appendix A. Supplementary data

Supplementary data to this article can be found online at https://doi.org/10.1016/j.biomaterials.2021.120686.

Fundings

This study was supported by JSPS KAKENHI Grant Numbers JP19K20670 (T.K.), JP19K12780 (H.T.) and JP17H03560 (I.T.).

Data availability

The raw/processed data required to reproduce these findings cannot be shared at this time as the data also forms part of an ongoing study.

References

[1] K. Blennow, M.J. de Leon, H. Zetterberg, Alzheimer's disease, Lancet 368 (2006) 387–403, https://doi.org/10.1016/S0140-6736(06)69113-7.

[2] J. Hardy, D.J. Selkoe, The amyloid hypothesis of Alzheimer's disease: progress and problems on the road to therapeutics, Science 297 (80) (2002) 353–356, https://doi.org/10.1126/science.1072994.

[3] D.J. Selkoe, J. Hardy, The amyloid hypothesis of Alzheimer's disease at 25 years, EMBO Mol. Med. 8 (2016) 595–608, https://doi.org/10.15252/emmm.201606210.

[4] U. Sengupta, A.N. Nilson, R. Kayed, EBioMedicine the role of amyloid- β oligomers in toxicity , propagation , and immunotherapy, EBIOM 6 (2016) 42–49, https://doi.org/10.1016/j.ebiom.2016.03.035.

[5] K. Ono, K. Hasegawa, H. Naiki, M. Yamada, Curcumin has potent anti-amyloidogenic effects for Alzheimer's β-amyloid fibrils in vitro, J. Neurosci. Res. 75 (2004) 742–750, https://doi.org/10.1002/jnr.20025.

[6] F. Yang, G.P. Lim, A.N. Begum, O.J. Ubeda, M.R. Simmons, S.S. Ambegaokar, P. Chen, R. Kayed, C.G. Glabe, S.A. Frautschy, G.M. Cole, Curcumin inhibits formation of amyloid β oligomers and fibrils, binds plaques, and reduces amyloid in vivo, J. Biol. Chem. 280 (2005) 5892–5901, https://doi.org/10.1074/jbc.M404751200.

[7] P. Maiti, T.C. Hall, L. Paladugu, N. Kolli, C. Learman, J. Rossignol, G.L. Dunbar, A comparative study of dietary curcumin, nanocurcumin, and other classical amyloid-binding dyes for labeling and imaging of amyloid plaques in brain tissue of 5×-familial Alzheimer's disease mice, Histochem. Cell Biol. 146 (2016) 609–625, https://doi.org/10.1007/s00418-016-1464-1.

[8] D. Yanagisawa, H. Taguchi, A. Yamamoto, N. Shirai, K. Hirao, I. Tooyama, Curcuminoid binds to amyloid-β_{1-42} oligomer and fibril, J. Alzheim. Dis. 24 (2011) 33–42, https://doi.org/10.3233/JAD-2011-102100.

[9] D. Yanagisawa, N. Shirai, T. Amatsubo, H. Taguchi, K. Hirao, M. Urushitani, S. Morikawa, T. Inubushi, M. Kato, F. Kato, K. Morino, H. Kimura, I. Nakano, C. Yoshida, T. Okada, M. Sano, Y. Wada, K. -n. Wada, A. Yamamoto, I. Tooyama, Relationship between the tautomeric structures of curcumin derivatives and their Aβ-binding activities in the context of therapies for Alzheimer's disease, Biomaterials 31 (2010) 4179–4185, https://doi.org/10.1016/j.biomaterials.2010.01.142.

[10] I. Tooyama, N.F. Ibrahim, L.W. Durani, H. Shahirah Hamezah, M.H.A. Damanhuri, W.Z.W. Ngah, H. Taguchi, D. Yanagisawa, Curcumin against Amyloid Pathology in Mental Health and Brain Composition, 2016, https://doi.org/10.1016/B978-0-12-802972-5.00023-8.

[11] W.B. Stine, K.N. Dahlgren, G.A. Krafft, M.J. LaDu, In vitro characterization of conditions for amyloid-β peptide oligomerization and fibrillogenesis, J. Biol. Chem. 278 (2003) 11612–11622, https://doi.org/10.1074/jbc.M210207200.

[12] S. Barghorn, V. Nimmrich, A. Striebinger, G. Krantz, P. Keller, B. Janson, M. Bahr, M. Schmidt, R.S. Bitner, J. Harlan, E. Barlow, U. Ebert, H. Hillen, Globular amyloid β-peptide1-42 oligomer - a homogenous and stable neuropathological protein in Alzheimer's disease, J. Neurochem. 95 (2005) 834–847, https://doi.org/10.1111/j.1471-4159.2005.03407.x.

[13] K. Murakami, Y. Horikoshi-Sakuraba, N. Murata, Y. Noda, Y. Masuda, N. Kinoshita, H. Hatsuta, S. Murayama, T. Shirasawa, T. Shimizu, K. Irie, Monoclonal antibody against the turn of the 42-residue amyloid β-protein at positions 22 and 23, ACS Chem. Neurosci. 1 (2010) 747–756, https://doi.org/10.1021/cn100072e.

[14] T. Umeda, S. Maekawa, T. Kimura, A. Takashima, T. Tomiyama, H. Mori, Neurofibrillary tangle formation by introducing wild-type human tau into APP transgenic mice, Acta Neuropathol. 127 (2014) 685–698, https://doi.org/10.1007/s00401-014-1259-1.

[15] T. Umeda, E.M. Ramser, M. Yamashita, K. Nakajima, H. Mori, M.A. Silverman, T. Tomiyama, Intracellular amyloid β oligomers impair organelle transport and induce dendritic spine loss in primary neurons, Acta Neuropathol. Commun. 3 (2015) 51, https://doi.org/10.1186/s40478-015-0230-2.

[16] H. Okuno, K. Mori, T. Jitsukawa, H. Inoue, S. Chiba, Convenient method for monitoring Aβ aggregation by quartz-crystal microbalance, Chem. Biol. Drug Des. 68 (2006) 273–275, https://doi.org/10.1111/j.1747-0285.2006.00446.x.

[17] J.L. Jankowsky, D.J. Fadale, J. Anderson, G.M. Xu, V. Gonzales, N.A. Jenkins, N. G. Copeland, M.K. Lee, L.H. Younkin, S.L. Wagner, S.G. Younkin, D.R. Borchelt, Mutant presenilins specifically elevate the levels of the 42 residue β-amyloid peptide in vivo: evidence for augmentation of a 42-specific γ secretase, Hum. Mol. Genet. 13 (2004) 159–170, https://doi.org/10.1093/hmg/ddh019.

[18] N. Naruse, H. Satooka, K. Todo, A. Nakanishi, H. Taguchi, Y. Mera, Oligomers imaging of amyloid-β1-42 by scanning tunneling microscopy, Jpn. J. Appl. Phys. 58 (2019), https://doi.org/10.7567/1347-4065/ab203b.

[19] K. Irie, New Diagnostic Method for Alzheimer ' S Disease Based on the Toxic Conformation Theory of Amyloid β, 2020, p. 19, https://doi.org/10.1080/09168451.2019.1667222.

[20] M. Ono, H. Saji, Molecular approaches to the treatment , prophylaxis , and diagnosis of alzheimer ' s Disease : novel PET/SPECT imaging probes for diagnosis of alzheimer, s Disease 344 (2012) 338–344, https://doi.org/10.1254/jphs.11R08FM.

[21] F. Panza, M. Lozupone, G. Logroscino, B.P. Imbimbo, A critical appraisal of amyloid-β-targeting therapies for Alzheimer disease, Nat. Rev. Neurol. 15 (2019) 73–88, https://doi.org/10.1038/s41582-018-0116-6.

[22] M. Tolar, S. Abushakra, M. Sabbagh, The path forward in Alzheimer's disease therapeutics: reevaluating the amyloid cascade hypothesis, Alzheimer's Dementia 16 (11) (2020) 1553–1560, https://doi.org/10.1016/j.jalz.2019.09.075.

[23] C.L. Teoh, D. Su, S. Sahu, S.W. Yun, E. Drummond, F. Prelli, S. Lim, S. Cho, S. Ham, T. Wisniewski, Y.T. Chang, Chemical fluorescent probe for detection of Aβ oligomers, J. Am. Chem. Soc. 137 (2015) 13503–13509, https://doi.org/10.1021/jacs.5b06190.

[24] Y. Li, D. Xu, A. Sun, S.L. Ho, C.Y. Poon, H.N. Chan, O.T.W. Ng, K.K.L. Yung, H. Yan, H.W. Li, M.S. Wong, Fluoro-substituted cyanine for reliable: in vivo labelling of

amyloid-β oligomers and neuroprotection against amyloid-β induced toxicity, Chem. Sci. 8 (2017) 8279–8284, https://doi.org/10.1039/c7sc03974c.

[25] Y. Li, J. Yang, H. Liu, J. Yang, L. Du, H. Feng, Y. Tian, J. Cao, C. Ran, Tuning the stereo-hindrance of a curcumin scaffold for the selective imaging of the soluble forms of amyloid beta species, Chem. Sci. 8 (2017) 7710–7717, https://doi.org/10.1039/c7sc02050c.

[26] J. Yang, F. Zeng, X. Li, C. Ran, Y. Xu, Y. Li, Highly specific detection of Aβ oligomers in early Alzheimer's disease by a near-infrared fluorescent probe with a "v-shaped" spatial conformation, Chem. Commun. 56 (2020) 583–586, https://doi.org/10.1039/c9cc08894f.

[27] G. Lv, A. Sun, M. Wang, P. Wei, R. Li, T. Yi, A novel near-infrared fluorescent probe for detection of early-stage Aβ protofibrils in Alzheimer's disease, Chem. Commun. 56 (2020) 1625–1628, https://doi.org/10.1039/c9cc09233a.

[28] I. Benilova, E. Karran, B. De Strooper, The toxic Aβ oligomer and Alzheimer's disease: an emperor in need of clothes, Nat. Neurosci. 15 (2012) 349–357, https://doi.org/10.1038/nn.3028.

[29] E.N. Cline, M.A. Bicca, K.L. Viola, W.L. Klein, The amyloid-β oligomer hypothesis: beginning of the third decade, J. Alzheim. Dis. 64 (2018) S567–S610, https://doi.org/10.3233/JAD-179941.